



KTN80 confers precision to microtubule severing by specific targeting of katanin complexes in plant cells

Chaofeng Wang^{1,2,†}, Weiwei Liu^{1,2,†}, Guangda Wang^{1,2,†} , Jun Li^{2,3}, Li Dong¹, Libo Han¹, Qi Wang¹, Juan Tian¹, Yanjun Yu¹, Caixia Gao³ & Zhaosheng Kong^{1,*} 

Abstract

The microtubule (MT)-severing enzyme katanin triggers dynamic reorientation of cortical MT arrays that play crucial functions during plant cell morphogenesis, such as cell elongation, cell wall biosynthesis, and hormonal signaling. MT severing specifically occurs at crossover or branching nucleation sites in living *Arabidopsis* cells. This differs from the random severing observed along the entire length of single MTs *in vitro* and strongly suggests that a precise control mechanism must exist *in vivo*. However, how katanin senses and cleaves at MT crossover and branching nucleation sites *in vivo* has remained unknown. Here, we show that the katanin p80 subunit KTN80 confers precision to MT severing by specific targeting of the katanin p60 subunit KTN1 to MT cleavage sites and that KTN1 is required for oligomerization of functional KTN80–KTN1 complexes that catalyze severing. Moreover, our findings suggest that the katanin complex in *Arabidopsis* is composed of a hexamer of KTN1–KTN80 heterodimers that sense MT geometry to confer precise MT severing. Our findings shed light on the precise control mechanism of MT severing in plant cells, which may be relevant for other eukaryotes.

Keywords katanin; microtubule severing; plant cortical microtubules; the p60 subunit; the p80 subunit

Subject Categories Cell Adhesion, Polarity & Cytoskeleton; Plant Biology

DOI 10.15252/embj.201796823 | Received 26 February 2017 | Revised 31 August 2017 | Accepted 8 September 2017 | Published online 4 October 2017

The EMBO Journal (2017) 36: 3435–3447

Introduction

Plant cells establish cortical microtubule (MT) arrays that are independent of centrosomes and closely aligned with the plasma membrane in a two-dimensional layer (Ehrhardt, 2008; Wasteneys & Ambrose, 2009; Shaw, 2013). During cell morphogenesis, plant

cortical MTs play a crucial role by providing tracks for cellulose synthase complexes in cellulose biosynthesis (Paredes *et al*, 2006; McFarlane *et al*, 2014; Watanabe *et al*, 2015; Li *et al*, 2016). Additionally, plant cortical MTs are also thought to act as sensors that respond to developmental and environmental stimuli via their dynamic reorganization (Nick, 2013). The majority of nascent MTs formed during remodeling are nucleated from the wall of the pre-existing MTs in either a branching or parallel fashion (Nakamura *et al*, 2010). Previously, we showed that the augmin complex recruits the γ -tubulin complex to pre-existing MTs where it triggers nascent MT nucleation (Liu *et al*, 2014). The fate of nascent MTs is usually associated with the MT-severing enzyme katanin complex, which severs daughter MTs at branching nucleation sites, after which the detached daughter MTs translocate via treadmilling to form new configuration of MT arrays (Nakamura *et al*, 2010).

Katanin is composed of a 60-kDa catalytic ATPase Associated with diverse cellular Activities (AAA) subunit and an 80-kDa WD-40 repeat-containing regulatory subunit (McNally & Vale, 1993; Roll-Mecak & McNally, 2010; Sharp & Ross, 2012). *In vitro*, the *Arabidopsis* p60 subunit KTN1 (also named KSS, Katanin Small Subunit) severs MTs along their entire length (Stoppin-Mellet *et al*, 2002, 2007). Negative staining electron microscopy showed that KTN1/KSS forms a hexamer ring structure (Stoppin-Mellet *et al*, 2007), consistent with the higher-order structure of its sea urchin homolog and another MT-severing enzyme, spastin (Hartman *et al*, 1998; Hartman & Vale, 1999; Roll-Mecak & Vale, 2008), through the conserved AAA⁺ domain in the presence of ATP. Notably, genetic studies have shown that KTN1 plays crucial roles in cell morphogenesis, cell wall mechanics, and hormonal signaling (Burk *et al*, 2001; Webb *et al*, 2002; Bouquin *et al*, 2003; Uyttewaal *et al*, 2012; Peaucelle *et al*, 2015). Intriguingly, in addition to its role in severing at branching nucleation sites (Nakamura *et al*, 2010), KTN1 was observed to be primarily recruited to MT crossover sites to initiate severing (Lindeboom *et al*, 2013; Zhang *et al*, 2013). MT severing plays central roles in driving the dynamic remodeling of cortical MT arrays during plant cell morphogenesis and environmental adaption,

¹ State Key Laboratory of Plant Genomics, Institute of Microbiology, Chinese Academy of Sciences, Beijing, China

² University of Chinese Academy of Sciences, Beijing, China

³ State Key Laboratory of Plant Cell and Chromosome Engineering, Institute of Genetics and Developmental Biology, Chinese Academy of Sciences, Beijing, China

*Corresponding author. Tel/Fax: +86 10 6480 6099; E-mail: zskong@im.ac.cn

[†] These authors contributed equally to this work

affecting processes, such as hormonal signaling, phototropic responses, and mechanical stress responses (Uyttewaald *et al*, 2012; Lindeboom *et al*, 2013; Roll-Mecak, 2013; Wightman *et al*, 2013; Sampathkumar *et al*, 2014; Peaucelle *et al*, 2015).

Unlike random severing along single MTs *in vitro*, live-cell observations showed that KTN1 is primarily recruited to MT crossovers and branching nucleation sites to trigger severing (Nakamura *et al*, 2010; Wightman *et al*, 2013; Zhang *et al*, 2013), strongly indicating the existence of a precise control mechanism for MT severing *in vivo*. However, it remains to be determined how severing is precisely triggered at MT crossovers and branching nucleation sites. In particular, how the p80 subunits participate in precise MT severing and in forming the katanin supercomplex *in vivo* has not yet been explored. Hence, the p80 subunit is the primary candidate for uncovering the enigma of precise MT severing. Here, we use live-cell imaging, genetic and biochemical approaches, to investigate the *in vivo* function of katanin p80 subunits in MT severing. We find that the p80 subunit is required for specific targeting of the p60 subunit to sites of MT severing. We also find that *de novo* assembly of the p60-p80 multimeric katanin supercomplex on MTs confers precise MT severing at crossover sites and branching nucleation sites in living *Arabidopsis* cells.

Results

Four KTN80s act redundantly to regulate anisotropic cell elongation during plant cell morphogenesis

The *Arabidopsis thaliana* genome has four loci encoding katanin p80 subunits, At1G11160, At1G61210, At5G08390, and At5G23430, which we designated the encoded katanin subunits KTN80.1, 2, 3, and 4, respectively. Among these, KTN80.1 and KTN80.2 fall into one subclade in the phylogenetic tree, and KTN80.3 and KTN80.4 belong to another subclade (Fig EV1A). Previous mass spectrometry assays identified KTN80.2 and KTN80.3 in microtubule-associated protein-enriched preparations (Hamada *et al*, 2013), and microarray analyses detected the transcripts of all four KTN80s (identified from the AtGenExpress database, <http://jsp.weigelworld.org/expviz/expviz.jsp>). KTN80.3 and KTN80.4 showed similar expression patterns, with high expression levels, whereas KTN80.1 and KTN80.2 showed relatively low expression levels (based on data from the AtGenExpress database). We further validated the expression patterns of the KTN80s by RT-PCR (Fig EV1B and C), and the results were consistent with the microarray data. Collectively, these results indicate that the four *Arabidopsis* KTN80s are expressed in all tissues examined and KTN80s may play redundant roles during development, together with the single p60 subunit encoded by KTN1.

To gain genetic insights into the *in vivo* function of KTN80s during development, we generated stable *ktn80.1 ktn80.2* (termed *ktn80.12*) and *ktn80.3 ktn80.4* (termed *ktn80.34*) double mutants using CRISPR/Cas9 genome editing technology (Fig 1A and B) (Wang *et al*, 2014). Those double mutants were further confirmed to be null because the frameshift insertions/deletions in the coding sequence resulted in premature stop codons (Fig 1C). However, the *ktn80.12* and *ktn80.34* double mutants grow normally, and they do not show obvious growth defects (Fig 1A and B). Thus, we next created *ktn80.1234* quadruple mutants by crossing the *ktn80.12* and

ktn80.34 double mutants (Fig 1A and B). Notably, the *ktn80.1234* quadruple mutants exhibited a severe dwarf phenotype, with smaller, rounder dark-green rosette leaves and wider, shorter petioles compared to wild type, as was also seen for the katanin p60 mutant *lue1* (Fig 1A and B). The *lue1* mutant is confirmed to be a KTN1 null allele, which contains a nonsense mutation in the fifth exon (at the 1,179-bp position), very close to the T-DNA insertion site in the *ktn1-2* null mutant (Bouquin *et al*, 2003; Nakamura *et al*, 2010). Collectively, the results indicate that the four KTN80s redundantly regulate anisotropic elongation during plant cell morphogenesis, and suggest that KTN80s function together with the p60 subunit KTN1 during development.

KTN80s function in precise MT severing at crossovers and branching nucleation sites

To explore whether the KTN80s contribute to MT severing, we made KTN80-GFP fusion constructs using the KTN80 genomic sequences, including the upstream promoter region, and found that these constructs fully complemented the *ktn80.1234* quadruple mutant (Fig EV2A). We next performed live-cell imaging using dual-labeled transgenic lines expressing both KTN80-GFPs and mCherry-TUB6 (β -tubulin 6, for labeling cortical MTs). In leaf epidermal pavement cells, KTN80s decorated the cortical MTs and appeared as discrete particles that remained immobile for various lengths of time before disappearing from the cortical MTs (Movies EV1 and EV2). Notably, most KTN80 particles specifically localized to either MT crossovers (~52%) or branching nucleation sites (~20%), and half led to successful MT severing at these sites (Fig 2A–E, Movies EV1 and EV2). The distribution and dynamic behavior of the KTN80s were comparable to those of the control p60 subunit KTN1 (Fig 2E and F), as recorded using a functional fusion of GFP-KTN1 that fully complements the *lue1* mutant phenotype (Fig EV2B). We found that severing of single MTs was negligible, with a frequency of approximately 1% for both KTN80s and KTN1 (Fig 2E). Taken together, these results indicate that KTN80s specifically function in MT severing at crossover and branching nucleation sites, further suggesting that KTN80s and KTN1 control precise MT severing through the formation of functional MT-severing complexes.

KTN80 quadruple mutant displays a complex cortical MT network with stable entanglements

To explore the cellular mechanisms associated with cell elongation defects in the *ktn80.1234* quadruple mutants, we analyzed the organization of MTs in mutant cells. Epidermal pavement cells in *ktn80.1234* quadruple mutant leaves displayed more complex MT networks with bent and long MTs at higher density, frequently forming stable entanglements, compared to the wild-type control (Fig 3A). Strikingly, epidermal petiole cells of the quadruple mutants exhibited net-like MT arrays, whereas the wild-type control showed well-aligned MT arrays (Fig 3B). The abnormal MT organization in the *ktn80.1234* quadruple mutant is reminiscent of that observed in the p60 mutant alleles, *fra2*, *lue1*, and *bot1* (Burk *et al*, 2001; Bouquin *et al*, 2003; Wightman *et al*, 2013). Taken together, these results indicate that the four KTN80s act redundantly to regulate cell elongation by modulating MT organization, possibly by manipulating MT severing.

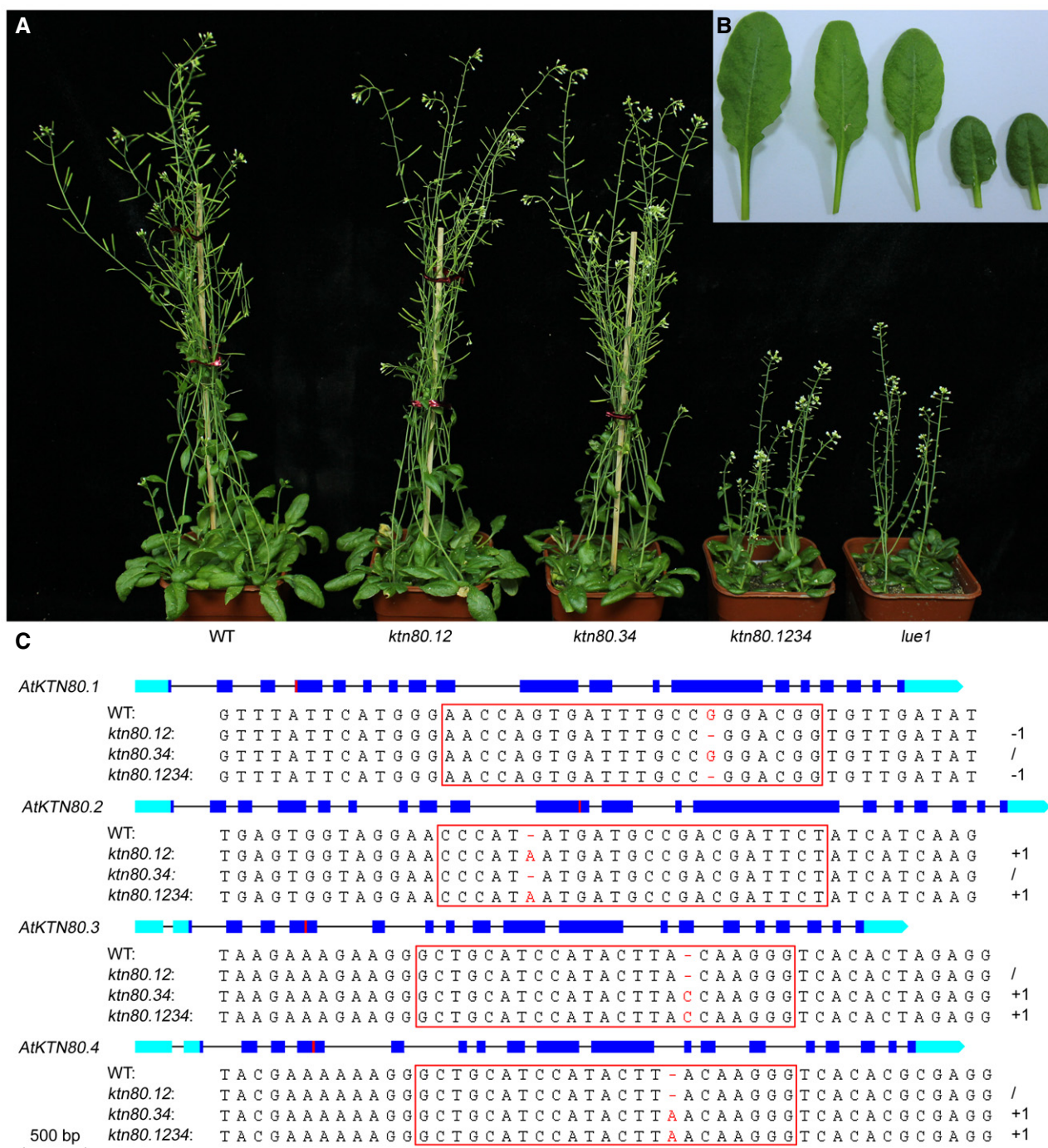


Figure 1. Generation, genetic identification, and phenotypic analysis of the *ktn80.1234* quadruple mutants.

A, B Phenotypic comparison of the wild-type control (Col-0), various *KTN80* knockout lines, and the *lue1* mutant. The *ktn80.12* and *ktn80.34* double mutants and *ktn80.1234* quadruple mutants were obtained via CRISPR/Cas9 genome editing technology. The order of representative rosette leaves shown in (B) is same as that in (A).

C The gene structures of *KTN80s* and the respective edited sites. The 5'-UTR and 3'-UTR are shown in light blue, CDS are shown in dark blue, boxes indicate exons, and lines indicate introns. Red bars in exons indicate the positions of sgRNA:Cas9 targets. The sgRNA:Cas9 targets are highlighted in red boxes, and the mutated sites are shown in red.

Loss of *KTN80* function results in the disruption of KTN1 recruitment and consequent abolishment of MT severing

To ascertain how the stable MT entanglements form, we compared MT dynamics in *ktn80.1234* quadruple mutant cells and wild-type

control cells. MT severing frequently occurs at either branching nucleation sites or crossover sites in control cells (Fig 3C, Movie EV3). MT severing at crossovers effectively eliminates discordant MTs in establishing a well-aligned MT array (Wightman & Turner, 2007; Wightman et al, 2013). When a single MT passes through an aligned array, many

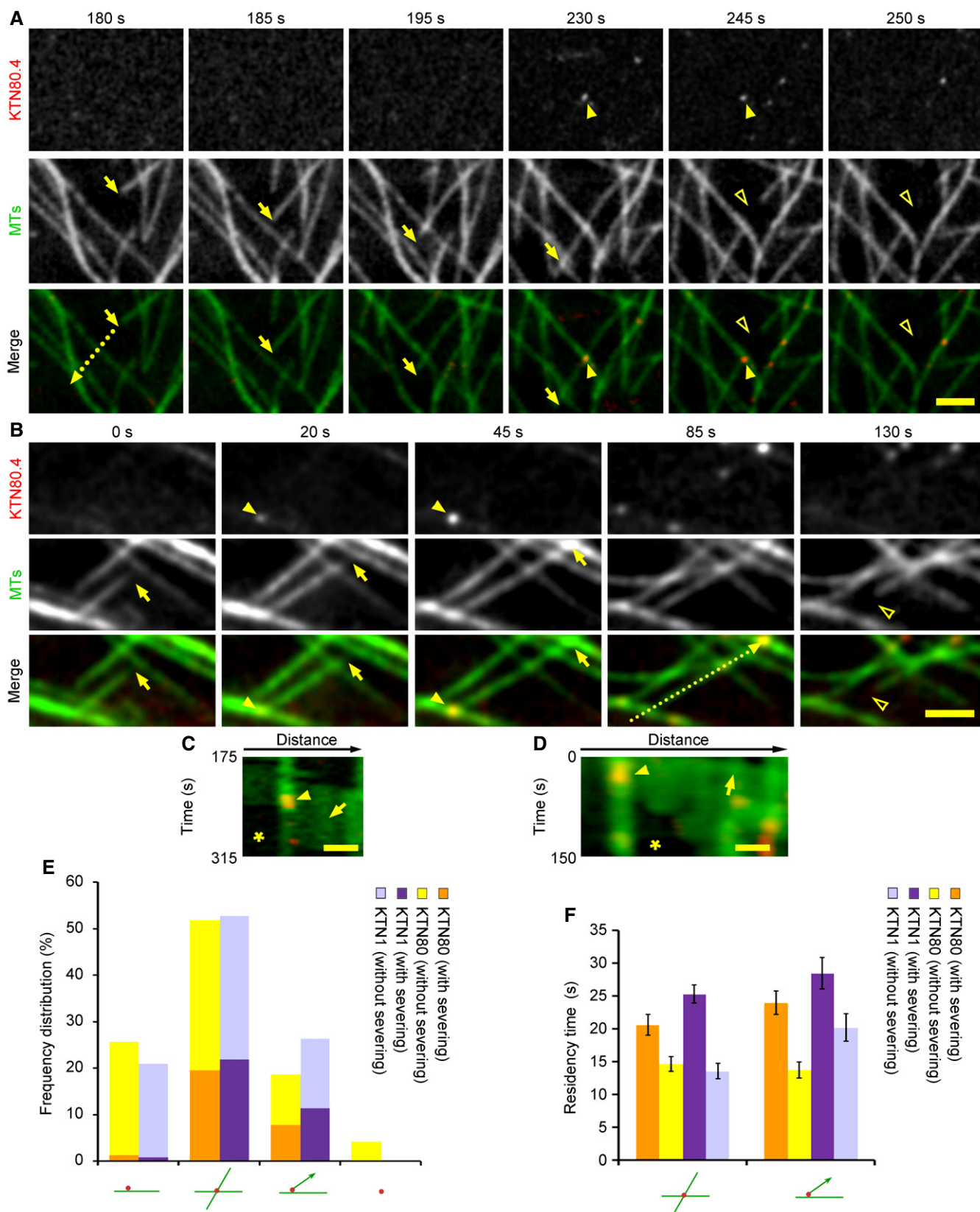


Figure 2.

Figure 2. KTN80s function in MT severing at crossovers and branching nucleation sites.

- A Time-lapse images showing that KTN80.4 is associated with MT severing at crossover sites. GFP-labeled KTN80.4 particles are pseudo-colored in red, and MTs (labeled with mCherry-TUB6) are shown in green. Yellow arrows track the growing plus end of the crossing MT. Yellow arrowheads indicate KTN80.4, which dwells at MT crossover sites. Hollow arrowheads indicate the crossing MT gets severed at the crossover site and the new plus end of the severed MT undergoes shrinkage. The dotted yellow line indicates the position and direction for the kymograph shown in (C). Scale bars, 2 μm . See also Movie EV1.
- B Time-lapse images showing that KTN80.4 is associated with MT severing at branching nucleation sites. Yellow arrows track the growing plus end of the nascent MT during branching nucleation. Yellow arrowheads indicate KTN80.4, which dwells at the branch nucleation site. Hollow arrowheads indicate the nascent MT gets severed at the branch nucleation site and the new minus end of the severed daughter MT undergoes shrinkage. The dotted yellow line indicates the position and direction for the kymograph shown in (D). Scale bars, 2 μm . See also Movie EV2.
- C Kymograph showing the severing event shown in (A). The green slope indicated by the yellow arrow illustrates the growth of the crossing MT, and the red patch indicated by the yellow arrowhead shows the short dwell time of KTN80.4. The asterisk indicates the loss of MT signal caused by severing of the crossing MT at the crossover site and subsequent shrinking of the new plus end of the severed MT. Scale bar, 1 μm .
- D Kymograph showing the severing event shown in (B). The green slope indicated by the yellow arrow illustrates the growth of the daughter MT of branching nucleation, and the red patch indicated by the yellow arrowhead shows the short dwell time of KTN80.4. The asterisk indicates the loss of MT signal caused by severing of the daughter MT at the branch nucleation site and subsequent shrinking of the minus end of the severed daughter MT. Scale bar, 1 μm .
- E Distribution of katanin (red dots) at cortical MTs (green lines) and associated MT-severing events. 528 KTN80-associated events from three cells and 331 KTN1-related events from three cells were collected for analysis, respectively.
- F Comparison of residency times of katanin during MT severing. 371 KTN80-associated events from three cells and 261 KTN1-related events from three cells were collected for analysis, respectively. Error bars indicate SEM.

Source data are available online for this figure.

crossovers are formed. In most cases, the invading (crossing) MT gets severed at the sites where it crosses other MTs and finally becomes fragmented or depolymerized (Fig 3C, Movie EV3). By contrast, no severing was observed at MT crossover sites in *ktn80.1234* quadruple mutant cells (2,612 μm^2 areas in three cells were examined over 5 min) (Fig 3C, Movie EV3). Consequently, MT crossovers remain stable for a long time and they accumulate to form the MT entanglements that characterize mutant cells (Fig 3A–C). We next monitored the behaviors of KTN1 in *ktn80.1234* quadruple mutant cells to gain further insight into the specific roles of KTN80 in MT severing *in vivo*. Notably, no GFP-KTN1 particles were observed to localize to MTs (Fig 3D, Movie EV4). We used a construct that co-expressed both GFP-KTN1 and mCherry-TUB6 (see Materials and Methods), and while we observed mCherry-labeled MTs, GFP-KTN1 was not seen in *ktn80.1234* quadruple mutant cells, although GFP-KTN1 expression was confirmed by Western blotting (Fig 3E). These results demonstrate that MT severing is completely abolished in the *ktn80.1234* quadruple mutants due to the impaired recruitment of KTN1 to MTs (3,388 μm^2 areas in four cells were examined over 5 min). These findings show that KTN80s are required to target katanin complexes to sites where MT severing occurs, and also suggest that KTN80s recruits KTN1 onto MTs during assembly of katanin supercomplexes.

KTN1 is dispensable for KTN80 localization, but KTN80 is required for proper targeting of katanin complexes *in vivo*

We next evaluated KTN80s in the *lue1* mutant background to clarify the spatial and temporal relationship of KTN1 and KTN80s to MT severing. We found that KTN80s were able to localize on MTs, primarily at MT crossovers and branching nucleation sites, but never initiated MT severing in *lue1* cells (Fig 4A, Movie EV5), unlike what we observed in the wild-type control (Fig 4A, Movie EV5). Quantitatively, the distribution and residency times of KTN80s puncta were comparable in *lue1* and wild-type cells (Fig 4B and C). *lue1* cells have more MT crossovers than do wild-type cells (Fig 4A, Movie EV5) but, after normalization, we found comparable frequencies (KTN80 puncta at MT crossovers per 100 $\mu\text{m}^2/\text{s}$ per crossover) of KTN80 recruitment between *lue1* and control cells (Fig 4D). Although the recruitment of KTN1 to MTs depends on

KTN80s (see Fig 3D), it was formally possible that KTN1 encodes a N-terminal truncated protein that interferes with or modifies katanin function in *lue1* cells. Therefore, we used CRISPR/Cas9 to generate a new *KTN1* null allele *ktn1-c1*, and we found that this new mutant shows identical growth defects, as those shown by *lue1*, *fra2* and *bot1* mutants (Fig EV3A and B). The *ktn1-c1* mutant contains a frameshift mutation at 22 bp from the start codon and it only encodes 7 amino acids of the N-terminal region of KTN1 plus 14 novel amino acids (Fig EV3B), indicating that it is an absolutely *KTN1* null allele. Subsequent observations further confirmed that MT severing is completely disrupted (3,134.08 μm^2 area in four cells were examined over 3 min), but with normal KTN80 behaviors in *ktn1-c1* cells (Fig EV3C, Movie EV6). These results show that loss of KTN1 does not affect KTN80 localization and behaviors, but KTN80 is required for KTN1 targeting, strongly indicating that KTN80 confers precision to MT severing.

The *Arabidopsis* katanin complex is likely a hexamer of KTN1–KTN80 heterodimers *in vivo*

We examined the physical interactions among katanin proteins using bimolecular fluorescence complementation (BiFC) assays in *Agrobacterium*-infiltrated *Nicotiana benthamiana* leaves to demonstrate the composition of the katanin supercomplex *in vivo*. Our results show that all four KTN80s strongly interact with KTN1. Strikingly, a YFP signal, which indicates KTN80/KTN1 interaction, decorates cortical MTs (Fig 5A), and crossover and branching nucleation sites have bright puncta (Fig 5A) that resemble the *in vivo* localization patterns of KTN1/KTN80s. By contrast, no physical interaction was detected in between the combinations of KTN80.1–KTN80.2, KTN80.2–KTN80.3, and KTN80.2–KTN80.4, and very weak interactions were observed in KTN80.1–KTN80.4 and KTN80.3–KTN80.4; among the combinations we tested, only KTN80.1–KTN80.3 showed stronger interaction (Fig 5B). Previous *in vitro* studies have shown that the sea urchin katanin-p60 can form a higher-order structure of a hexamer ring through the conserved AAA⁺ domain in the presence of ATP, like another MT-severing enzyme, spastin (Hartman et al, 1998; Hartman & Vale, 1999; Roll-Mecak & Vale, 2008). Likewise, the *Arabidopsis* KTN1/KSS was shown to form a ring structure

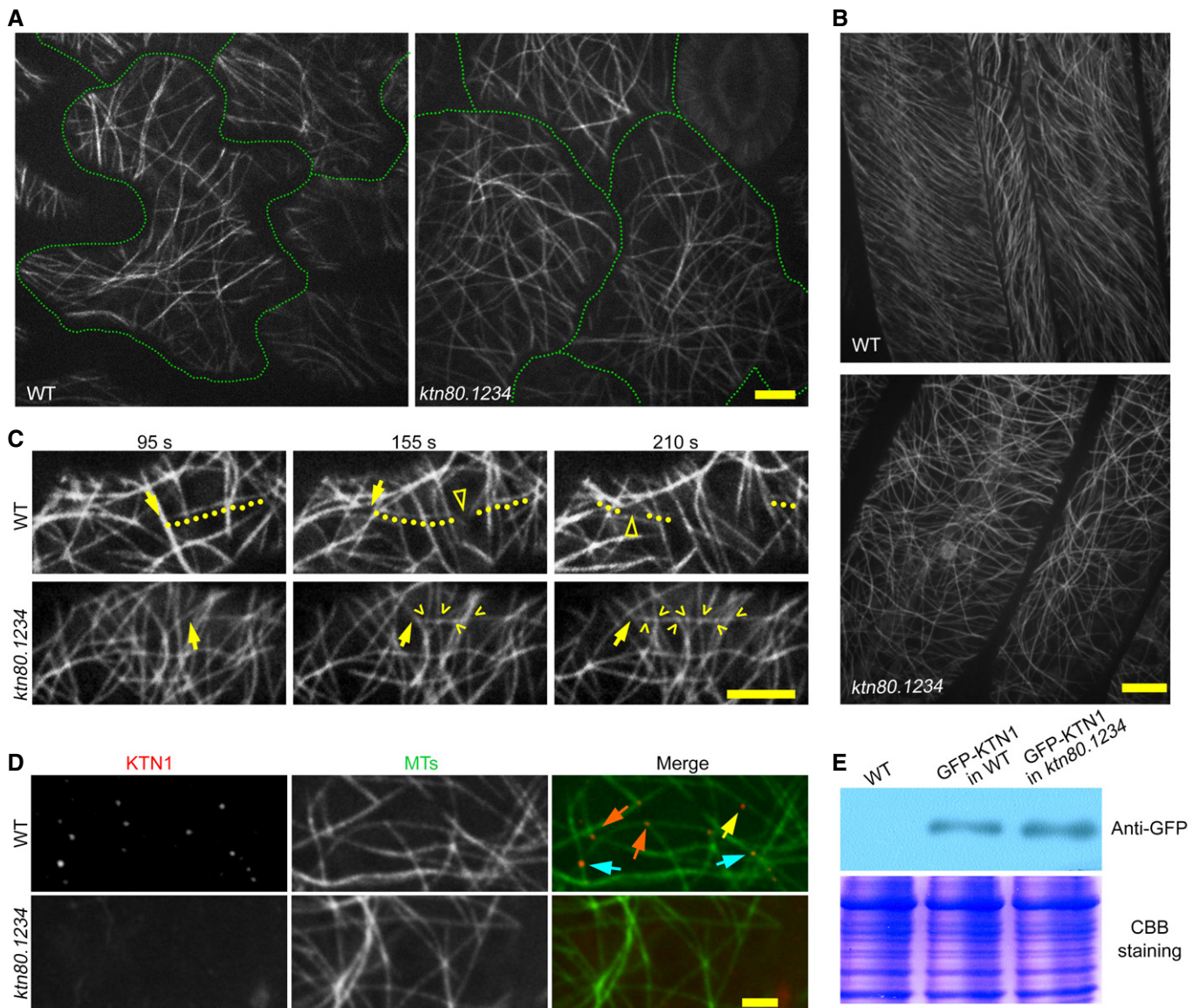


Figure 3. The *ktn80.1234* quadruple mutants display abnormal MT organization, abolished MT severing, and disrupted recruitment of KTN1.

- A Comparison of cortical MT (labeled with GFP-TUB6) patterns in epidermal pavement cells between the control and the *ktn80.1234* quadruple mutant. Cell outlines are highlighted with green dotted lines. Scale bar, 5 μ m.
- B Comparison of cortical MT (GFP-TUB6) patterns in epidermal petiole cells (shown in part) between the control and the *ktn80.1234* quadruple mutant. Scale bar, 5 μ m.
- C MT severing is completely abolished in epidermal pavement cells of *ktn80.1234* quadruple mutant cells, compared with the control cells. Yellow arrows track the growing ends of the crossing MT, which forms many crossovers with other MTs. In control cells, the crossing MT gets severed at the crossover site (marked with yellow hollow arrowheads) and consequently becomes fragmented or depolymerized. Dotted yellow lines depict the intact crossing MT or MT fragments caused by severing. In *ktn80.1234* quadruple mutant cells, no severing was observed, and the MT crossovers (indicated by yellow open arrowheads) keep stable for a long time. Scale bars, 5 μ m. See also Movie EV3.
- D The recruitment of GFP-labeled KTN1 (pseudo-colored in red) to MTs (mCherry-TUB6; pseudo-colored in green) is completely disrupted in *ktn80.1234* quadruple mutant cells, compared with the wild-type control. In control cells, cyan arrows indicate crossover-localized KTN1, orange arrows indicate KTN1 landing at branching nucleation sites, and KTN1 on single MTs is marked with the yellow arrow. Scale bar, 2 μ m. See also Movie EV4.
- E Western blot indicates that GFP-KTN1 fusion proteins could be detected by the anti-GFP monoclonal antibodies in *ktn80.1234* quadruple mutants. Coomassie Brilliant Blue (CBB) staining of SDS-PAGE gels as the loading control.

Source data are available online for this figure.

of similar size and sever MTs *in vitro* (Stoppin-Mellet et al, 2007). Indeed, structural prediction demonstrated a hexameric ring conformation for KTN1 (Fig EV4). Perhaps KTN80 targets KTN1–KTN80

heterodimers to MT crossover and branching nucleation sites where KTN1 triggers formation of a hexamer of these heterodimers to achieve MT severing. We used a co-immunoprecipitation assay (see

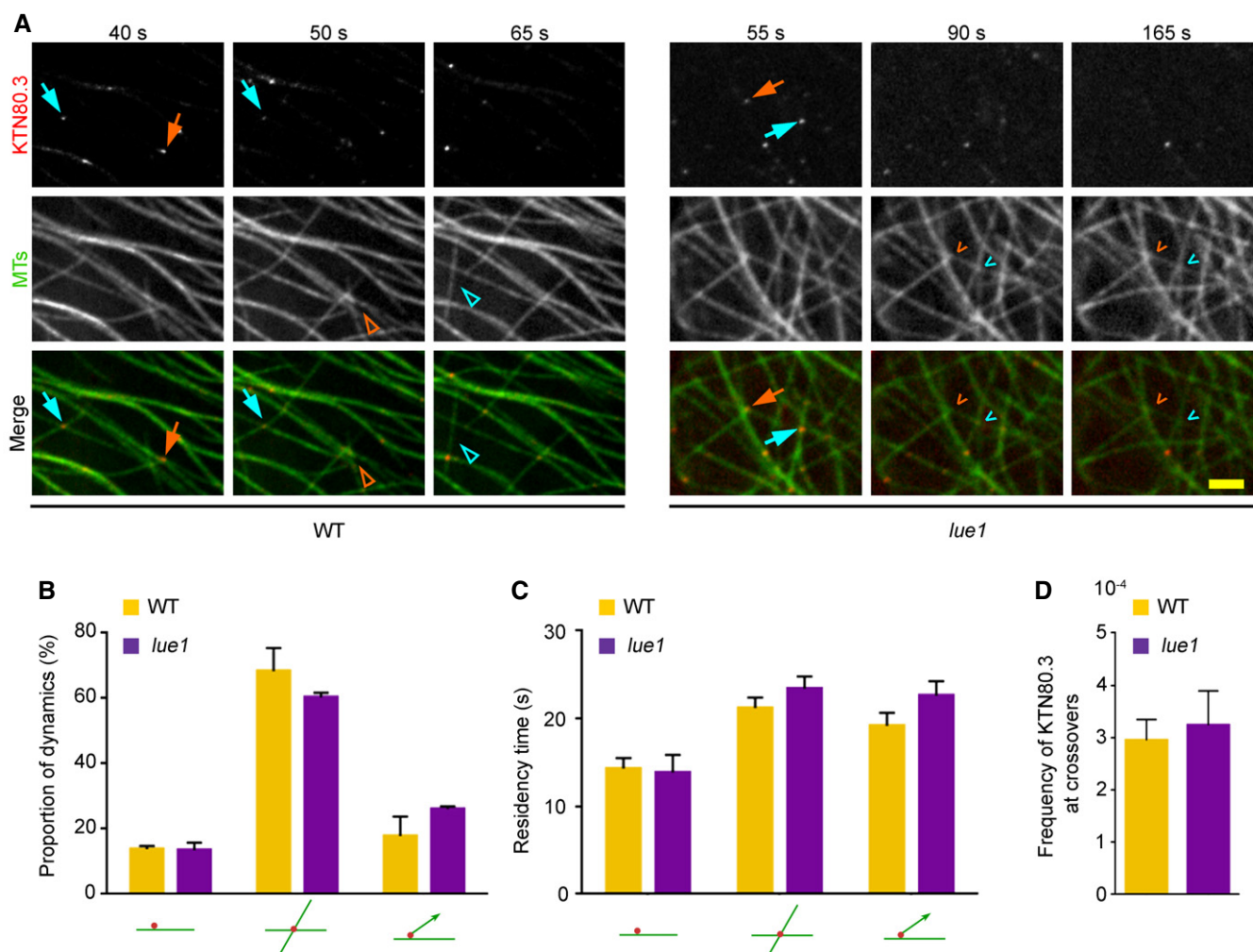


Figure 4. KTN1 is dispensable for KTN80 targeting and dynamics.

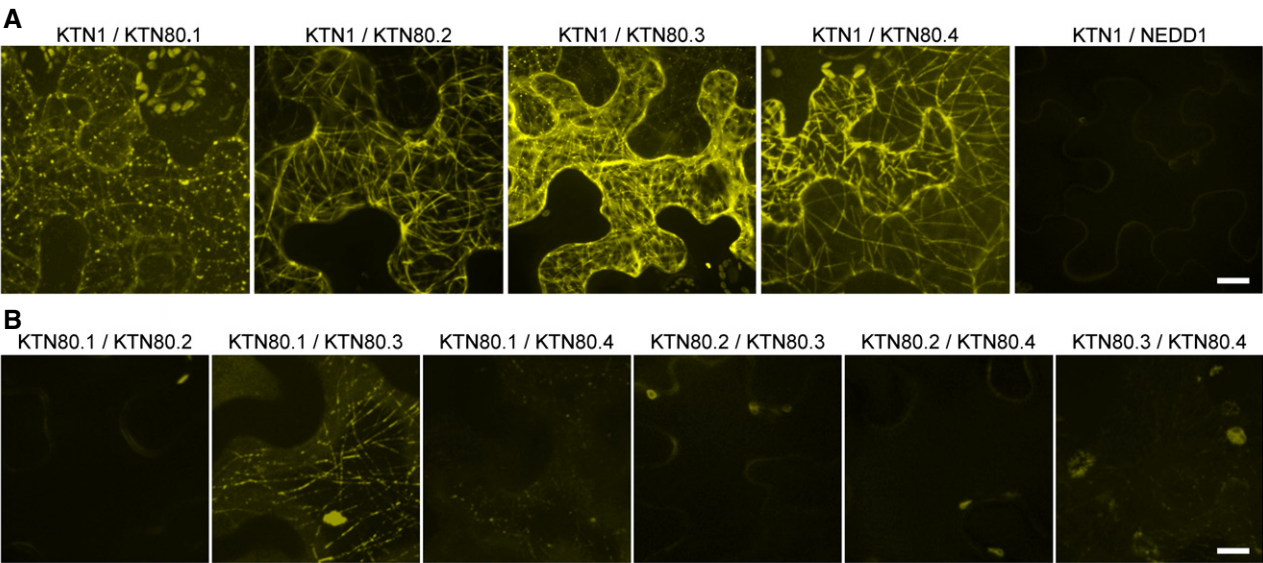
- A Comparison of the localization of GFP-labeled KTN80.3 (red particles) at cortical MTs (mCherry-TUB6, pseudo-colored in green) between the *lue1* cells and the wild-type control. Cyan arrows indicate crossover-localized KTN80.3. Orange arrows indicate KTN80.3 landing at branching nucleation sites. In control cells, KTN80.3 triggers MT severing at crossovers (marked with cyan hollow arrowheads) and branching nucleation sites (marked with orange hollow arrowheads), respectively. In *lue1* cells, MTs never get severed, and the MT configuration of the indicated crossover (cyan open arrowheads) and the branching nucleation (orange open arrowheads) keeps stable for a long time. Scale bar, 2 μ m. See also Movie EV5.
- B Comparison of the proportions of KTN80.3 that show different residences at three representative sites, between *lue1* cells and the control. 514 KTN80.3-associated events in three wild-type cells and 372 KTN80.3-associated events in three *lue1* cells were collected for analysis both (B) and (C). Error bars indicate SD.
- C Comparison of residency times of KTN80.3 particles, which are distributed at three representative sites, cortical MT between *lue1* and control cells. Error bars indicate SEM.
- D Comparison of relative landing frequency (expressed as observed landings per 100 μ m²/s per crossover) of KTN80.3, which localizes at MT crossover sites, between *lue1* and control cells; 350 KTN80.3-associated events were detected in 3,225 μ m² areas of three wild-type cells over 12 min, and 225 KTN80.3-associated events were detected in 1,637 μ m² areas of three *lue1* cells over 10 min. Error bars indicate SD.

Source data are available online for this figure.

Materials and Methods) without added ATP and found that each of the four KTN80s co-precipitated with KTN1, but not the other KTN80s, indicating robust formation of KTN1–KTN80 heterodimers under physiological conditions (Fig 5C). When we added ATP to co-immunoprecipitation assay, KTN80s could be co-purified with each other (Fig 5D). These results indicate that KTN1 initially forms a heterodimer with one of the four KTN80s before the higher-order structure takes shape, and that the *Arabidopsis* katanin complex is likely a hexamer of KTN1–KTN80 heterodimers.

Mixed types of KTN80s form a functional supercomplex with KTN1 to perform MT severing

We investigated co-localization patterns among katanin proteins to further uncover the composition of the katanin supercomplex *in vivo*. Observations in living cells showed extensive co-localization of KTN1 and KTN80s (Fig 6A, Movie EV7), and also between various KTN80–KTN80 pairs (Fig 6B, Movie EV7). These observations indicate that mixed types of KTN80s form a



C Mass spectrometry results of AtKTNs' interaction (-ATP)

Hits	Bait																	
	KTN80.1			KTN80.2			KTN80.3			KTN80.4			KTN1			Reference		
	#pep	#spe	cov(%)	#pep	#spe	cov(%)	#pep	#spe	cov(%)	#pep	#spe	cov(%)	#pep	#spe	cov(%)	#pep	#spe	cov(%)
KTN80.1	52	133	54.75	—	—	—	—	—	—	—	—	—	—	—	—	—	—	—
KTN80.2	—	—	—	88	423	67.74	—	—	—	—	—	—	—	—	—	—	—	—
KTN80.3	—	—	—	—	—	—	62	322	65.67	—	—	—	17	47	31.59	—	—	—
KTN80.4	—	—	—	—	—	—	—	—	—	31	65	49.28	6	22	14.11	—	—	—
KTN1	22	27	41.87	37	89	58.13	49	243	57.93	28	45	47.42	41	477	58.13	—	—	—
GFP	31	110	84.43	40	304	89.47	41	445	89.47	25	71	75.23	36	225	86.38	—	—	—

#pep: number of peptides #spe: number of spectra cov(%): Coverage (%)

D Mass spectrometry results of AtKTNs' interaction (+ATP)

Hits	Bait																	
	KTN80.1			KTN80.2			KTN80.3			KTN80.4			KTN1			Reference		
	#pep	#spe	cov(%)	#pep	#spe	cov(%)	#pep	#spe	cov(%)	#pep	#spe	cov(%)	#pep	#spe	cov(%)	#pep	#spe	cov(%)
KTN80.1	31	63	41.63	—	—	—	9	18	11.26	—	—	—	—	—	—	—	—	—
KTN80.2	—	—	—	13	18	13.99	—	—	—	—	—	—	7	7	9.75	—	—	—
KTN80.3	3	4	4.89	24	53	38.50	43	259	53.99	13	19	20.62	26	52	40.64	—	—	—
KTN80.4	—	—	—	20	18	33.37	7	13	6.94	28	127	42.11	22	61	36.00	—	—	—
KTN1	32	153	48.18	52	458	69.41	44	260	57.93	42	204	58.89	56	601	73.23	—	—	—
GFP	24	109	75.23	30	396	76.16	37	550	86.07	34	366	83.28	32	473	73.68	—	—	—

#pep: number of peptides #spe: number of spectra cov(%): Coverage (%)

Figure 5. Physical interactions among katanin proteins in the katanin supercomplex *in vivo*.

A BiFC confocal image showing a strong interaction between KTN1 and KTN80s. NEDD1, which functions in MT nucleation, was used as the negative control. Scale bar, 20 μm.

B BiFC confocal image showing no or very weak interaction among KTN80s. Scale bar, 20 μm.

C, D Immunoprecipitation and mass spectrometry analysis of the KTN80–KTN1 interaction either in ATP-free preparations (**C**) or in the presence of ATP (**D**). GFP-tagged KTN80 lines were used for immunoprecipitation using GFP-Trap_A kit (Chromotek). Wild-type Col-0 was used as negative control (Reference). The bait is highlighted in gray.

supercomplex with KTN1, and further suggest that different KTN80s may simultaneously act in MT severing with KTN1. Furthermore, live-cell observations showed that, in each of the four GFP-tagged KTN80 marker lines with comparable MT densities and severing frequencies (Fig 6C), most MT-severing events were linked to the presence of GFP-labeled particles, as was true for KTN1 (Fig 6D). The percentages are comparable among KTN80.2, KTN80.3, KTN80.4, and KTN1, but KTN80.1

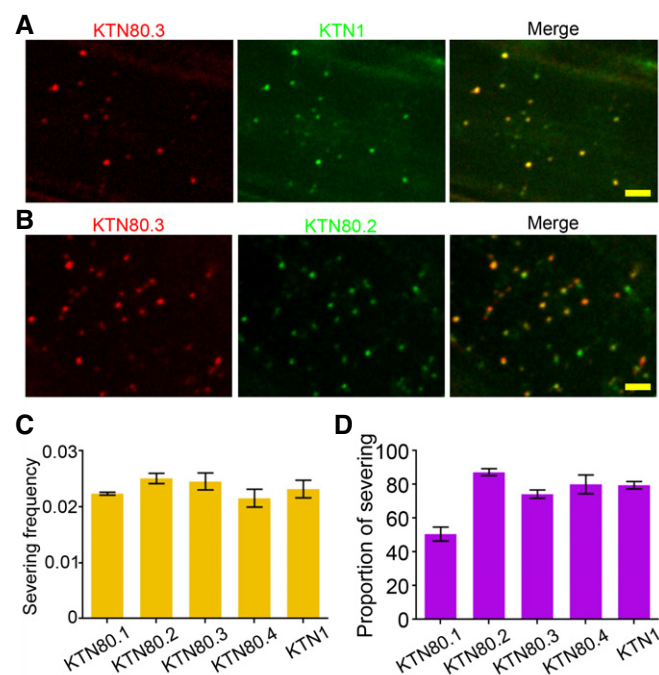


Figure 6. Co-localization of katanin proteins and simultaneous involvement of different KTN80s in individual MT-severing events.

- A Co-localization of TagRFP-labeled KTN80.3 (red particles) with GFP-labeled KTN1 (green particles). Among 383 KTN80.3 particles and 402 KTN1 particles, 356 particles were co-localized and three cells were examined. Scale bar, 2 μm . See also Movie EV7.
- B Co-localization of TagRFP-labeled KTN80.3 (red particles) with GFP-labeled KTN80.2 (green particles). Among 437 KTN80.3 particles and 356 KTN80.2 particles, 179 particles were co-localized and three cells were examined. Scale bar, 2 μm . See also Movie EV7.
- C Comparison of the severing frequencies (expressed as observed severing per 100 $\mu\text{m}^2/\text{s}$) of the selected epidermal pavement cells in different GFP-labeled KTN1/80 lines.
- D Comparison of the percentages of severing events associated with GFP-labeled particles against all the examined severing events in different GFP-labeled KTN1/80 lines.

Data information: The statistical analysis in (C) and (D) was conducted in the following way. For KTN80.1, 2,668 μm^2 areas were examined over 11 min; KTN80.2, 1,928 μm^2 , 8 min; KTN80.3, 3,225 μm^2 , 12 min; KTN80.4, 2,910 μm^2 , 15 min; KTN1, 2,554 μm^2 , 12 min. Error bars indicate SD. Source data are available online for this figure.

showed a relatively lower occupancy percentage (Fig 6D), which is correlated with its low expression level (see Fig EV1B and C). These results suggest that four different KTN80s simultaneously participate in an individual MT-severing event and that mixed types of KTN80s form a functional supercomplex with KTN1 to perform MT severing *in vivo*.

Since all four KTN80s are expressed, there would be four types of KTN1–KTN80 heterodimers in a single cell. Our data favor a model in which the katanin supercomplex is a hexamer of KTN1–KTN80 heterodimers of mixed types (Fig 7). In addition, the four types of KTN1–KTN80 heterodimers can complement each other, and thus, only the KTN80 quadruple mutants showed severe growth defects, as observed in the KTN1 null mutant. This suggests that the four different KTN80s are functionally equivalent.

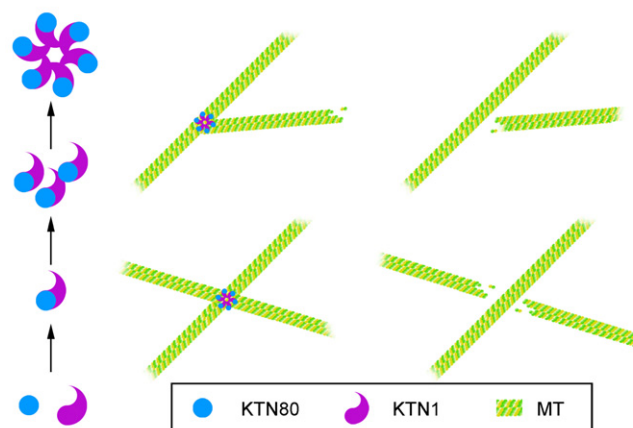


Figure 7. A schematic model depicting the formation of katanin complexes and precise MT severing in living *Arabidopsis* cells.

The katanin p60 subunit KTN1 and p80 subunit KTN80 exist as a KTN1–KTN80 heterodimer in the cytosol; KTN80 determines the precise targeting of KTN1–KTN80 heterodimers to MTs, primarily at crossover and branching nucleation sites. KTN1 further triggers the oligomerization of the mixed types of KTN1–KTN80 heterodimers to *de novo* form a hexamer of katanin supercomplex at MTs. KTN1 forms the core module of the hexamer to perform MT-severing activities.

Discussion

Our findings provide the first live-cell evidence that all four *Arabidopsis* KTN80s function in MT severing at both crossovers and branching nucleation sites and play redundant roles during development. We showed that KTN80 is required for specific targeting of katanin complexes and KTN1 is required for oligomerization in forming functional katanin complexes. We also showed that precise MT severing depends on the orchestration of katanin complexes and the MT geometry of crossover and branching nucleation sites.

KTN80 defines the precision of MT severing via specific targeting of katanin complexes

Although extensive *in vitro* assays have been developed for different species, the result varies depending on the experimental system. In sea urchin, human, *Drosophila* and *Arabidopsis*, the katanin p60 subunit is sufficient to sever MTs (Hartman *et al*, 1998; McNally *et al*, 2000; Stoppin-Mellet *et al*, 2007; Diaz-Valencia *et al*, 2011), while both the p60 and p80 subunits are required for MT severing in *Caenorhabditis elegans* and *Tetrahymena* (McNally *et al*, 2006; Sharma *et al*, 2007). Thus far, the exact roles of p60 and p80 in MT severing remain unclear. On the other hand, prior work has shown that katanin regulates neuron development *in vivo*. For instance, defective MT severing is associated with neuronal abnormalities, including Alzheimer's disease where abnormal aggregation of the MT-associated tau protein might interfere with its role in preventing excess MT severing (Qiang *et al*, 2006; Eom *et al*, 2014; Mao *et al*, 2014). Additionally, katanin is essential for both male and female fertility via modulating the assembly of meiotic spindles (McNally *et al*, 2006; Loughlin *et al*, 2011; O'Donnell *et al*, 2012; Smith *et al*, 2012). However, the complexity of MT networks, which are often organized into thick bundles inside neurons and spindles, has made

katanin-mediated MT severing difficult to evaluate in living animal cells (Roll-Mecak, 2013). So far, the cortical MT array in *Arabidopsis* is the only system in which microtubule severing events can be directly observed. In contrast to *in vitro* observations showing that KTN1/KSS randomly severs single MTs along the length (Stoppin-Mellet et al, 2002, 2007), live-cell imaging demonstrated that MT severing specifically occurs either at MT crossover sites or branching nucleation sites, raising an open question how MT severing is precisely controlled. Intriguingly, our live-cell observations, for the first time, revealed that four KTN80s function in MT severing at crossovers and branching nucleation sites (see Fig 2). Moreover, we successfully generated *ktn80.1234* quadruple mutants and further demonstrated that MT severing is abolished in *ktn80.1234* quadruple cells (see Fig 3). Most importantly, we observed that the recruitment of KTN1 to MTs is completely impaired in *ktn80.1234* quadruple cells (see Fig 3), but KTN80s behaviors are unaltered in *KTN1* null cells (see Fig 4). Therefore, our findings reveal that KTN80 determines the site where katanin-mediated MT severing occurs via specific targeting of KTN1 to MTs, primarily at crossover sites and branching nucleation sites.

Orchestration of katanin complexes with the specific MT geometries confers precise MT severing in living *Arabidopsis* cells

Our live-cell observations (see Figs 3, 4, 5A and B, and 6), together with co-immunoprecipitation data (see Fig 5C and D), indicate that KTN80 determines precise targeting of KTN1–KTN80 heterodimers to MTs, primarily at crossover and branching nucleation sites. KTN1 further triggers oligomerization to form a hexamer of KTN1–KTN80 heterodimers at MTs *de novo*. KTN1 forms the core module of the hexamer to perform MT-severing activities as suggested by negative staining electron micrographs and structural modeling (Hartman et al, 1998; Stoppin-Mellet et al, 2007; Roll-Mecak & Vale, 2008), and KTN80s attach the six radiating arms of the KTN1 hexamer and stretch outwards to provide multiple binding sites to MTs (see the Model in Fig 7). Accordingly, the specific MT geometries at crossover and branching nucleation sites probably provide multivalent binding interfaces between KTN80s and MTs, further facilitating the stabilization and conformational activation of katanin supercomplexes (see the Model in Fig 7). Most prior *in vitro* work that examined katanin cleavage of MTs utilized preparations that had individual MTs in solution (McNally et al, 2000; Stoppin-Mellet et al, 2002; Diaz-Valencia et al, 2011). However, a recent *in vitro* study examined how immobilized orthogonal MT arrays were severed by purified MEI-1/MEI-2 (the katanin p60/p80 in *C. elegans*), and they observed that the rate of MT severing at MT crossovers is five times faster than it is on individual MTs (McNally et al, 2014). This *in vitro* work, together with our *in vivo* experiments, suggests that the preferred substrate of katanin complexes are sites where MTs interact with other MTs. Our findings are also consistent with an *in vitro* study showing a 1:1 stoichiometry MEI-1:MEI-2 within the katanin complex, which was suggested to be a hexamer of MEI-1/MEI-2 heterodimers (Joly et al, 2016). Based on the physical interaction between the N-terminal microtubule interacting and trafficking domain of p60 and the C-terminus of p80, the crystal structure of the mouse p60N/p80C heterodimer was recently resolved, providing the structural basis for formation of the p60/p80 heterodimer (Jiang et al, 2017). Even so, further *in vitro*

reconstruction of the katanin supercomplex and cryo-EM observations would likely strengthen this model.

Structural analysis indicates a MT-severing mechanism by which the KTN1 AAA domain binds to the C-terminal tail of tubulin through the central pore of the AAA hexamer (Roll-Mecak & Vale, 2008). Perhaps the central pore of the AAA hexamer of KTN1 recognizes lattice defects at MT crossovers and branching nucleation sites and this is followed by severing. This possibility is supported by an *in vitro* study showing that *Drosophila* katanin-p60 severs MT at sites of damaged lattice (Diaz-Valencia et al, 2011). Other recent work showed that MTs that cross other MTs exhibit a higher abundance of GTP-like islands in their defective or stressed regions and that these GTP-like islands, when recognized by rescue factors like CLIP-170 or the CLASPs, stabilize MTs at crossovers (de Forges et al, 2016). Notably, an *in vivo* study in *Arabidopsis* showed that SPIRAL2 moves along MTs but accumulates at crossover sites to prevent KTN1-mediated severing (Wightman et al, 2013). This work provides clues for identifying additional proteins that negatively regulate precise MT severing, although the physical and biochemical nature of the lattice defects at MT crossovers and branching nucleation sites are still unknown.

Our findings provide important insight into the molecular and cellular mechanisms of precise MT severing in living plant cells. This work has important implications for understanding MT severing in other eukaryote systems because the katanin p60/p80 complex is conserved and for developing new therapies in precision for the many diseases related to MT severing.

Materials and Methods

Plant materials and growth conditions

Arabidopsis thaliana ecotype Columbia (Col-0) was used as the genetic background in this study. The *lue1* allele in the Col-0 background was selected for analysis (accession number is CS9531 in the *Arabidopsis* Biological Resource Center). The mCherry-labeled MTs (mCherry-TUB6) marker line was described in our previous studies (Liu et al, 2014; Tian et al, 2015). Various cross combinations (GFP-labeled KTN80 lines and the mCherry-TUB6 line; the *lue1* mutant and GFP-labeled KTN80 lines; the GFP-KTN1 line and the KTN80.3-TagRFP line; GFP-KTN1 and mCherry-TUB6 dual-labeling line in *ktn80.1234* quadruple mutant background; GFP-KTN80.3 and mCherry-TUB6 dual-labeled line in the *lue1* background; the KTN80.3-TagRFP marker line and the GFP-labeled KTN80 lines) were performed to produce materials to observe the dynamics of katanin complexes and MTs.

Plant growth conditions and *Agrobacterium tumefaciens*-mediated transformation procedures were as described previously (Liu et al, 2014; Tian et al, 2015). The first or second true leaves in 2-week-old seedlings grown on soil were used for live-cell imaging of most observations. Anther filaments dissected from flowers during anthesis were used for observing co-localization among katanin proteins.

Generation of GFP/TagRFP-tagged KTN1/KTN80 lines

To obtain stable transgenic *Arabidopsis* lines expressing fluorescent markers for live-cell imaging, such as GFP-labeled KTN1,

GFP-labeled KTN80s, and TagRFP-labeled KTN80.3, construction strategies were as described in detail in our previous studies (Liu et al, 2014; Tian et al, 2015). Briefly, the Phusion high-fidelity DNA polymerase (New England Biolabs, Beverly, MA, USA) was used to amplify all the required gene products. Fusion PCR was applied to get the GFP (or TagRFP) fusions with the genes of interest, and Gateway technology was applied to get the final expression constructs. GFP-tagged KTN1 and GFP-tagged KTN80s were introduced into the binary vector pEarleyGate302 and pEarleyGate303 respectively, and the fusion of TagRFP-tagged KTN80.3 was introduced into the binary vector pGWB659. All these expression constructs were used with genomic sequences driven by their native promoters, respectively. Among these, the 950-bp upstream fragment from the translation initiation codon ATG was selected as the promoter for *KTN1*, and the 1,200-bp, 1,184-bp, 1,647-bp, and 1,038-bp upstream fragments from the translation initiation codon ATG were used as promoters of *KTN80.1*, *KTN80.2*, *KTN80.3*, and *KTN80.4*, respectively.

To facilitate the screening of dual-labeling marker lines in different genetic backgrounds, we also made the *mCherry-TUB6/GFP-KTN1* dual expression construct. First, the fusions of *mCherry-TUB6* and *GFP-KTN1* were amplified from *P_{TUB6}*: *mCherry-TUB6* and *P_{KTN1}*: *GFP-KTN1*, using primer pairs T6-K1(TUB6)-F/T6-K1(TUB6)-R and T6-K1(KTN1)-F/T6-K1(KTN1)-R, respectively. Second, the resulting PCR fragments were cloned into the pENTR/D-TOPO vector to get the Entry1 and Entry2 clones. Finally, both the Entry1 and Entry2 vectors were digested by *FseI* and *AvrII*, and further ligation reactions were conducted between the gel-purified fragments containing the *mCherry-TUB6* fusion and the *GFP-KTN1* fusion. The resulting Entry 3 clone was delivered into pEarleyGate302 by recombination reaction to get the final *mCherry-TUB6/GFP-KTN1* dual expression construct. The primers are listed in Table EV1.

RT-PCR assays

Total RNA was extracted from *Arabidopsis* (Col-0) fruits, flowers, leaves, shoots, and roots using the Rapid EASYspin plant RNA extraction kit (Biomed), respectively. Two micrograms of total RNA for each sample was used for reverse transcription with the SuperScript III First-Strand Synthesis System (Invitrogen) with oligo(dT) primers. The PCR amplification reactions were performed as described previously (Liu et al, 2014). *UBQ5* (At3G62250) was used as the reference gene. Primers for RT-PCR are listed in Table EV1.

Generation of *KTN80* quadruple mutants and the *ktn1-c1* null mutant

To simultaneously knock out the four KTN80-encoding genes *KTN80.1* (At1g11160), *KTN80.2* (At1g61210), *KTN80.3* (At5g08390), and *KTN80.4* (At5g23430), we first generated the *ktn80.12* double mutants and the *ktn80.34* double mutants using the CRISPR/Cas9 genome editing technology. The genomic sequences of *At5g08390* and *At5g23430* are highly similar to each other; therefore, we designed one single guide RNA (sgRNA) site C1 (GCTGCATCCAT ACTTACAA) targeting both *KTN80.3* and *KTN80.4*. Two DNA oligos OAt5g-1F/OAt5g-1R were synthesized and annealed, and then, the resulting product was inserted into *BsaI*-linearized *pHEE2A-TRI* to

get the final multiplex vector *pHEE2A-TRI-At5gC1*. For assembly of the two sgRNA sites (C3: AACCAGTGATTGCGGGGA targeting *KTN80.1* and C6: ATATGATGCCGACGATTCT targeting *KTN80.2*), the PCR fragment was amplified from *pCBC-DT1T2* with primers D1-C3BsF, D1-C3F0, D1-C6R0, and D1-C6BsR. The PCR product was purified and digested with *BsaI*, and then ligated into *BsaI*-linearized *pHEE2A-TRI* to get the final multiplex vector *pHEE2A-TRI-At1gC3C6*.

The *ktn80.12* double and *ktn80.34* double mutant lines were screened by PCR/restriction enzyme (PCR/RE) assay, and confirmed by sequencing, as described in the previous study (Wang et al, 2015). Then, the KTN80 quadruple mutant lines were obtained from a cross between *ktn80.12* double and *ktn80.34* double mutants, and further confirmed as previously described. Moreover, we predicted the genome-wide potential off-target sites for sgRNA C1, C3, and C6 using the CasOT tool (<http://www.rgenome.net/cas-offinder/>). No off-target site with three nucleotide mismatches to the recognition site was found for sgRNA C3 and sgRNA C6, whereas two off-target sites were identified for sgRNA C1 (Table EV2). We further found no mutation at these two off-target sites by sequencing.

To knock out the KTN1-encoding gene (At1g80350), we employed the CRISPR/Cas9 genome editing technology using a YAO promoter-driven system (Yan et al, 2015). A single guide RNA (sgRNA) site (GGGAAGTAGTAATTCGTTAG) was first designed. Two DNA oligos KTN1(CRISPR)-F/KTN1(CRISPR)-R were synthesized and annealed, and the resulting product was inserted into *BsaI*-linearized *AtU6-26-sgRNA-SK* to achieve the entry vector *AtU6-26-sgRNA-SK-KTN1*. Then the entry vector *AtU6-26-sgRNA-SK-KTN1* was digested with *NheI* and *SpeI* to get a ~642-bp sgRNA cassette-KTN1 and further ligation reaction was conducted between sgRNA cassette-KTN1 and *SpeI*-linearized binary vector *pCAMBIA1300-pYAO:Cas9*, which was introduced into *Arabidopsis* Col-0. The *ktn1-c1* lines were screened by PCR/restriction enzyme (PCR/RE) assay with primers KTN1(test)-F/KTN1(test)-R, and confirmed by sequencing, as described in our previous study (Wang et al, 2015). The detailed primers are listed in Tables EV1 and EV2.

Spinning disk confocal microscopy and image analysis

Live-cell imaging was carried out under a spinning disk confocal microscope (UltraView VoX, PerkinElmer, Beaconsfield, Buckinghamshire, UK) equipped with the Yokogawa Nipkow CSU-X1 spinning disk scanner, Hamamatsu EMCCD 9100-13, Nikon TiE inverted microscope with the Perfect Focus System. Acquired images were processed and analyzed using Volocity (PerkinElmer), Image J (<http://rsbweb.nih.gov/ij/>), MetaMorph (Molecular Devices, Sunnyvale, CA, USA), as described previously (Liu et al, 2014; Tian et al, 2015). The plugins “enhance contrast” and “subtract background” of ImageJ were used to reduce the noise of the images. The walking average plugin (http://valelab.ucsf.edu/~nstuurman/IJplugins/Running_ZProjector.html) was used to reduce the noise in time-lapse series.

Affinity purification, mass spectrometry, and immunoblotting assays

Total protein of fresh leaves (5 g) from 2-week-old plants was extracted with 5 ml extraction buffer [50 mM Tris-HCl, pH 7.5,

150 mM NaCl, 20% (v/v) glycerol, 2% (v/v) Triton X-100, 1 mM EDTA, 1 × Complete protease inhibitor cocktail (Roche), and 1 mM PMSF (phenylmethanesulfonyl fluoride)] and incubated with GFP-Trap_A kit (Chromotek) for 30 min at 4°C. Beads were washed three times with wash buffer (50 mM Tris-HCl, pH 7.5, 150 mM NaCl, 20% (v/v) glycerol, 0.1% (v/v) Triton X-100, 1 mM EDTA, pH 8.0, 1 × Complete protease inhibitor cocktail, and 1 mM PMSF). To facilitate the stabilization of the KTN1/KTN80 supercomplex, 250 μM ATP was added in extraction buffer, wash buffer, and elution buffer. To identify co-purified proteins, the immunoprecipitates were separated in 10% SDS-polyacrylamide gels and stained with GelCode Blue Safe protein stain (Thermo Scientific). The excised gel was digested with trypsin and subjected to LC-MS/MS (Beijing Qinglian Biotech Co., Ltd., China). Mass spectra were analyzed using Proteome Discoverer1.4 (Thermo Scientific) with the *Arabidopsis* protein database (http://www.arabidopsis.org/download_files/Sequences/TAIR10_blastsets/TAIR10_seq_20110103_representative_gene_model_updated). GFP-KTN1 proteins were extracted from Col-0 and *ktn80.1234* plants expressing the GFP-KTN1 fusion, and Col-0 non-transformants were used as the negative control. Anti-GFP monoclonal antibodies (Sigma, USA) were used to detect GFP-KTN1. Secondary antibodies were: goat anti-mouse IgG H&L (HRP)-conjugated antibody (Abcam, UK). Western blot signals were developed using a chemiluminescent detection kit (Millipore, MA01821, USA).

Bimolecular fluorescence complementation assay

The serial pSAT1 vectors *pSAT1-nEYFP-C1-DQ168995*, *pSAT1-cEYFP-C1-B-DQ168996*, *pSAT1-nEYFP-N1-DQ169001*, and *pSAT1-cEYFP-N1-DQ169000* were used as BiFC Gateway vectors to generate *nEYFP-cDNA*, *cEYFP-cDNA*, *cDNA-nEYFP*, and *cDNA-cEYFP* expression constructs. The cDNA of *KTN1* with *EcoRI* and *XmaI* sites was amplified using the Phusion DNA polymerase with high-fidelity (New England Biolabs), and then cloned into *pSAT1 BiFC* vectors using ClonExpress II One-Step Cloning Kit (Vazyme Biotech Co., Ltd.) according to the manufacturer's instructions. Expression constructs for the four *KTN80s* were obtained by the same method as for *KTN1*.

For BiFC experiments, the expression constructs were transformed into *A. tumefaciens* (strain C58C1) cells. The resulting C58C1 transformants were suspended in solution of 10 mM MgCl₂, 1 mM MES, and 150 μM acetosyringone. The mixtures were incubated at room temperature for at least 3 h without shaking and co-infiltrated into leaves of 3-week-old *N. benthamiana*. At 48 h after incubation, fluorescent signals were acquired by confocal laser scanning microscopy. The unfused protein cEYFP or nEYFP was used as the negative control.

Expanded View for this article is available online.

Acknowledgements

We thank Dr. Steven W. L'Hernault (Emory University) and Dr. Long Miao (Institute of Biophysics, Chinese Academy of Sciences), for critical comments on the manuscript. We also thank Dr. Tao Wan in Dr. George F. Gao's group (Institute of Microbiology, Chinese Academy of Sciences) for structural prediction of KTN1 model. We appreciate Dr. Qi Xie (Institute of Genetics and Developmental Biology, Chinese Academy of Sciences) for the gift of the YAO promoter-driven CRISPR/Cas9 system. We appreciate Dr. Yunhai Li and Dr.

Na Li (Institute of Genetics and Developmental Biology, Chinese Academy of Sciences) for the assistance in immunoprecipitation, and Beijing Qinglian Biotech Co., Ltd. in the mass spectrometric analysis. We appreciate Dr. Jian Ye (Institute of Microbiology, Chinese Academy of Sciences) for the gift of the BiFC vectors. We are grateful to Ms. Yao Wu and Dr. Lei Su (Institute of Microbiology, Chinese Academy of Sciences) for providing technical assistance and training service. We also appreciate the technical support of the UltraView Vox system from Lei Jiao (PerkinElmer). This study was supported by the National Science Foundation of China under Grant # 31571378 and # 31501088, by the startup fund of "One Hundred Talents" program of the Chinese Academy of Sciences and by the grants from the State Key Laboratory of Plant Genomics.

Author contributions

CW and WL devised and performed most experiments. GW analyzed the data, prepared figures and videos, and designed the working model. JL conducted plasmid construction for CRISPR-Cas9 knockout constructs and provided guidance for screening *KTN80* double and quadruple mutants. LD conducted affinity purification and mass spectrometry. LH, QW, JT, and YY provided essential materials or technical assistances. CG supervised target design for CRISPR-Cas9 gene editing and revised the article. ZK conceived the project, interpreted the data, and wrote and revised the article with input from all authors.

Conflict of interest

The authors declare that they have no conflict of interest.

References

- Bouquin T, Mattsson O, Naested H, Foster R, Mundy J (2003) The *Arabidopsis* lue1 mutant defines a katanin p60 ortholog involved in hormonal control of microtubule orientation during cell growth. *J Cell Sci* 116: 791–801
- Burk DH, Liu B, Zhong R, Morrison WH, Ye ZH (2001) A katanin-like protein regulates normal cell wall biosynthesis and cell elongation. *Plant Cell* 13: 807–827
- Diaz-Valencia JD, Morelli MM, Bailey M, Zhang D, Sharp DJ, Ross JL (2011) *Drosophila* katanin-60 depolymerizes and severs at microtubule defects. *Biophys J* 100: 2440–2449
- Ehrhardt DW (2008) Straighten up and fly right: microtubule dynamics and organization of non-centrosomal arrays in higher plants. *Curr Opin Cell Biol* 20: 107–116
- Eom TY, Stanco A, Guo J, Wilkins G, Deslauriers D, Yan J, Monckton C, Blair J, Oon E, Perez A, Salas E, Oh A, Ghukasyan V, Snider WD, Rubenstein JL, Anton ES (2014) Differential regulation of microtubule severing by APC underlies distinct patterns of projection neuron and interneuron migration. *Dev Cell* 31: 677–689
- de Forges H, Pilon A, Cantaloube I, Pallandre A, Haghir-Gosnet AM, Perez F, Pous C (2016) Localized mechanical stress promotes microtubule rescue. *Curr Biol* 26: 3399–3406
- Hamada T, Nagasaki-Takeuchi N, Kato T, Fujiwara M, Sonobe S, Fukao Y, Hashimoto T (2013) Purification and characterization of novel microtubule-associated proteins from *Arabidopsis* cell suspension cultures. *Plant Physiol* 163: 1804–1816
- Hartman JJ, Mahr J, McNally K, Okawa K, Iwamatsu A, Thomas S, Cheesman S, Heuser J, Vale RD, McNally FJ (1998) Katanin, a microtubule-severing protein, is a novel AAA ATPase that targets to the centrosome using a WD40-containing subunit. *Cell* 93: 277–287

- Hartman JJ, Vale RD (1999) Microtubule disassembly by ATP-dependent oligomerization of the AAA enzyme katanin. *Science* 286: 782–785
- Jiang K, Rezabkova L, Hua S, Liu Q, Capitani G, Altelaar AFM, Heck AJR, Kammerer RA, Steinmetz MO, Akhmanova A (2017) Microtubule minus-end regulation at spindle poles by an ASPM-katanin complex. *Nat Cell Biol* 19: 480–492
- Joly N, Martino L, Gigant E, Dumont J, Pintard L (2016) Microtubule-severing activity of the AAA⁺ ATPase katanin is essential for female meiotic spindle assembly. *Development* 143: 3604–3614
- Li S, Bashline L, Zheng Y, Xin X, Huang S, Kong Z, Kim SH, Cosgrove DJ, Gu Y (2016) Cellulose synthase complexes act in a concerted fashion to synthesize highly aggregated cellulose in secondary cell walls of plants. *Proc Natl Acad Sci USA* 113: 11348–11353
- Lindeboom JJ, Nakamura M, Hibbel A, Shundiyak K, Gutierrez R, Ketelaar T, Emons AM, Mulder BM, Kirik V, Ehrhardt DW (2013) A mechanism for reorientation of cortical microtubule arrays driven by microtubule severing. *Science* 342: 1245533
- Liu T, Tian J, Wang G, Yu Y, Wang C, Ma Y, Zhang X, Xia G, Liu B, Kong Z (2014) Augmin triggers microtubule-dependent microtubule nucleation in interphase plant cells. *Curr Biol* 24: 2708–2713
- Loughlin R, Wilbur JD, McNally FJ, Nedelec FJ, Heald R (2011) Katanin contributes to interspecies spindle length scaling in *Xenopus*. *Cell* 147: 1397–1407
- Mao CX, Xiong Y, Xiong Z, Wang Q, Zhang YQ, Jin S (2014) Microtubule-severing protein katanin regulates neuromuscular junction development and dendritic elaboration in *Drosophila*. *Development* 141: 1064–1074
- McFarlane HE, Doring A, Persson S (2014) The cell biology of cellulose synthesis. *Annu Rev Plant Biol* 65: 69–94
- McNally FJ, Vale RD (1993) Identification of katanin, an ATPase that severs and disassembles stable microtubules. *Cell* 75: 419–429
- McNally KP, Bazirgan OA, McNally FJ (2000) Two domains of p80 katanin regulate microtubule severing and spindle pole targeting by p60 katanin. *J Cell Sci* 113(Pt 9): 1623–1633
- McNally K, Audhya A, Oegema K, McNally FJ (2006) Katanin controls mitotic and meiotic spindle length. *J Cell Biol* 175: 881–891
- McNally K, Berg E, Cortes DB, Hernandez V, Mains PE, McNally FJ (2014) Katanin maintains meiotic metaphase chromosome alignment and spindle structure *in vivo* and has multiple effects on microtubules *in vitro*. *Mol Biol Cell* 25: 1037–1049
- Nakamura M, Ehrhardt DW, Hashimoto T (2010) Microtubule and katanin-dependent dynamics of microtubule nucleation complexes in the acentrosomal *Arabidopsis* cortical array. *Nat Cell Biol* 12: 1064–1070
- Nick P (2013) Microtubules, signalling and abiotic stress. *Plant J* 75: 309–323
- O'Donnell L, Rhodes D, Smith SJ, Merriner DJ, Clark BJ, Borg C, Whittle B, O'Connor AE, Smith LB, McNally FJ, de Kretser DM, Goodnow CC, Ormandy CJ, Jamsai D, O'Bryan MK (2012) An essential role for katanin p80 and microtubule severing in male gamete production. *PLoS Genet* 8: e1002698
- Paredes AR, Somerville CR, Ehrhardt DW (2006) Visualization of cellulose synthase demonstrates functional association with microtubules. *Science* 312: 1491–1495
- Peaucelle A, Wightman R, Hofte H (2015) The control of growth symmetry breaking in the *Arabidopsis* hypocotyl. *Curr Biol* 25: 1746–1752
- Qiang L, Yu W, Andreadis A, Luo M, Baas PW (2006) Tau protects microtubules in the axon from severing by katanin. *J Neurosci* 26: 3120–3129
- Roll-Mecak A, Vale RD (2008) Structural basis of microtubule severing by the hereditary spastic paraplegia protein spastin. *Nature* 451: 363–367
- Roll-Mecak A, McNally FJ (2010) Microtubule-severing enzymes. *Curr Opin Cell Biol* 22: 96–103
- Roll-Mecak A (2013) Botany. Shining light at microtubule crossroads. *Science* 342: 1180–1181
- Sampathkumar A, Krupinski P, Wightman R, Milani P, Berquand A, Boudaoud A, Hamant O, Jonsson H, Meyerowitz EM (2014) Subcellular and supracellular mechanical stress prescribes cytoskeleton behavior in *Arabidopsis* cotyledon pavement cells. *Elife* 3: e01967
- Sharma N, Bryant J, Wloga D, Donaldson R, Davis RC, Jerka-Dziadosz M, Gaertig J (2007) Katanin regulates dynamics of microtubules and biogenesis of motile cilia. *J Cell Biol* 178: 1065–1079
- Sharp DJ, Ross JL (2012) Microtubule-severing enzymes at the cutting edge. *J Cell Sci* 125: 2561–2569
- Shaw SL (2013) Reorganization of the plant cortical microtubule array. *Curr Opin Plant Biol* 16: 693–697
- Smith LB, Milne L, Nelson N, Eddie S, Brown P, Atanassova N, O'Bryan MK, O'Donnell L, Rhodes D, Wells S, Napper D, Nolan P, Lalanne Z, Cheeseman M, Peters J (2012) KATNAL1 regulation of sertoli cell microtubule dynamics is essential for spermiogenesis and male fertility. *PLoS Genet* 8: e1002697
- Stoppin-Mellet V, Gaillard J, Vantard M (2002) Functional evidence for *in vitro* microtubule severing by the plant katanin homologue. *Biochem J* 365: 337–342
- Stoppin-Mellet V, Gaillard J, Timmers T, Neumann E, Conway J, Vantard M (2007) *Arabidopsis* katanin binds microtubules using a multimeric microtubule-binding domain. *Plant Physiol Biochem* 45: 867–877
- Tian J, Han L, Feng Z, Wang G, Liu W, Ma Y, Yu Y, Kong Z (2015) Orchestration of microtubules and the actin cytoskeleton in trichome cell shape determination by a plant-unique kinesin. *Elife* 4: e09351
- Uyttewaal M, Burian A, Alim K, Landrein B, Borowska-Wykret D, Dedieu A, Peaucelle A, Ludynia M, Traas J, Boudaoud A, Kwiatkowska D, Hamant O (2012) Mechanical stress acts via katanin to amplify differences in growth rate between adjacent cells in *Arabidopsis*. *Cell* 149: 439–451
- Wang Y, Cheng X, Shan Q, Zhang Y, Liu J, Gao C, Qiu JL (2014) Simultaneous editing of three homoeoalleles in hexaploid bread wheat confers heritable resistance to powdery mildew. *Nat Biotechnol* 32: 947–951
- Wang ZP, Xing HL, Dong L, Zhang HY, Han CY, Wang XC, Chen QJ (2015) Egg cell-specific promoter-controlled CRISPR/Cas9 efficiently generates homozygous mutants for multiple target genes in *Arabidopsis* in a single generation. *Genome Biol* 16: 144
- Wasteneys GO, Ambrose JC (2009) Spatial organization of plant cortical microtubules: close encounters of the 2D kind. *Trends Cell Biol* 19: 62–71
- Watanabe Y, Meents MJ, McDonnell LM, Barkwill S, Sampathkumar A, Cartwright HN, Demura T, Ehrhardt DW, Samuels AL, Mansfield SD (2015) Visualization of cellulose synthases in *Arabidopsis* secondary cell walls. *Science* 350: 198–203
- Webb M, Jouannic S, Foreman J, Linstead P, Dolan L (2002) Cell specification in the *Arabidopsis* root epidermis requires the activity of ECTOPIC ROOT HAIR 3—a katanin-p60 protein. *Development* 129: 123–131
- Wightman R, Turner SR (2007) Severing at sites of microtubule crossover contributes to microtubule alignment in cortical arrays. *Plant J* 52: 742–751
- Wightman R, Chomici G, Kumar M, Carr P, Turner SR (2013) SPIRAL2 determines plant microtubule organization by modulating microtubule severing. *Curr Biol* 23: 1902–1907
- Yan L, Wei S, Wu Y, Hu R, Li H, Yang W, Xie Q (2015) High-efficiency genome editing in *Arabidopsis* using YAO promoter-driven CRISPR/Cas9 system. *Mol Plant* 8: 1820–1823
- Zhang Q, Fishel E, Bertroche T, Dixit R (2013) Microtubule severing at crossover sites by katanin generates ordered cortical microtubule arrays in *Arabidopsis*. *Curr Biol* 23: 2191–2195